**Rare Metal Materials and Engineering**
Volume 53, Issue 1, January 2024
Available online at www.rmme.ac.cn

Science Press

**Cite this article as**: Pu Yongliang, Qian Yiqi, Liu Yuxin, et al. Thermal Stability and Crystallization Behavior of Zr-Al-Ni-Cu-Ag Metallic Glasses with Multicomponent Replacement[J]. Rare Metal Materials and Engineering, 2024, 53(01): 8-16. DOI: 10.12442/j.issn.1002-185X.20230569.

ARTICLE

# Thermal Stability and Crystallization Behavior of Zr-Al-Ni-Cu-Ag Metallic Glasses with Multicomponent Replacement

**Pu Yongliang**[1], **Qian Yiqi**[1], **Liu Yuxin**[1], **Liu Cong**[2], **Ding Jing**[3], **Zhu Shengli**[4,5]

*[1] School of Materials Science and Engineering, Lanzhou Jiaotong University, Lanzhou 730070, China; [2] School of Materials Science and Engineering, Hebei University of Technology, Tianjin 300130, China; [3] School of Energy and Machinery, Dezhou University, Dezhou 253023, China; [4] School of Materials Science and Engineering, Tianjin University, Tianjin 300350, China; [5] Tianjin Key Laboratory of Composite and Functional Materials, Tianjin 300350, China*

**Abstract:** In order to improve the thermal stability and to obtain a large supercooled liquid region of metal glasses, the $Zr_{65-x}(Al_{0.21}Ni_{0.29}Cu_{0.04}Ag_{0.46})_{35+x}$ ($x$=0, 7.5, 15.0, 22.5) metallic glasses were investigated. The effects of component concentrations on the thermal stability, heat-induced precipitate phases, and mechanical properties were analyzed. Results show that with increasing the component concentrations, the peak position of the broad diffraction pattern shifts towards higher angles, indicating the occurrence of glass transition phenomenon. With increasing the glass transition temperature ($T_g$) and crystallization temperature ($T_x$), the liquidus temperature ($T_l$) is decreased, leading to decrease in the temperature difference (namely supercooled liquid region, $\Delta T_x$) between $T_x$ and $T_g$ and resulting in the increase in reduced glass transition range ($T_{rg}$). Additionally, the nucleation activation energy ($E_x$) and the growth activation energy ($E_{p1}$) are increased with increasing the solute concentration. The primary crystal changes from the combination of tetragonal $Zr_2Ni$, $Zr_2$(Cu, Ag), ZrAg, and hexagonal $Zr_5Al_3$ phases into the single tetragonal ZrAg phase. The Vickers hardness is also increased with increasing the solute concentration. In this research, a novel metallic glass, $Zr_{65-x}(Al_{0.21}Ni_{0.29}$-$Cu_{0.04}Ag_{0.46})_{35+x}$ ($x$=7.5), is developed, which presents a large $\Delta T_x$ of 141 K, high thermal stability, and strong crystallization resistance. This research adopting the multicomponent replacement strategy is of great significance to improve the thermal stability of metallic glasses.

**Key words:** metallic glass; thermal stability; crystallization behavior; microstructure; Vickers hardness

Multicomponent metallic glasses attract much attention due to their excellent properties, such as high strength, high hardness, extensive elastic limit, and good corrosion resistance[1–4]. However, the prerequisite for the possession of these excellent properties is that the alloy must have high glass formation ability (GFA). Thus, the composition design of amorphous alloy is crucial. Inoue et al[5] proposed three fundamental criteria for conventional metallic glasses: (1) the system should comprise more than three elements; (2) there should be a substantial difference in the ratios of atomic sizes (approximately 12% or more) of the three primary constituent elements; (3) negative heats of mixing should be observed among the three primary constituent elements.

Recently, a subclass of multicomponent metallic glasses has been elaborated: the clustered glassy phase alloys[1]. These alloys have remarkable thermal stability and crystallization resistance, and the majority of the glass phases can remain even after the initial thermal peak vanishes. The clustered metallic glasses commonly have a supercooled liquid region ($\Delta T_x$) and multiple exothermic peaks in their differential scanning calorimetry (DSC) curves. Icosahedral phase tends to precipitate at the first exothermic peak during annealing. Nonetheless, the X-ray diffraction (XRD) pattern shows minimal change after annealing process due to the small size of precipitates. Moreover, in order to synthesize the clustered glassy alloys with high thermal stability, introducing solute elements with positive mixing heats and significant atomic size mismatches is also a promising method[3]. The presence of

Received date: September 12, 2023
Foundation item: Lanzhou Jiaotong University-Tianjin University Joint Innovation Foundation of China (2021051); Young Scholars Science Foundation of Lanzhou Jiaotong University (2019002)
Corresponding author: Zhu Shengli, Ph. D., Professor, School of Materials Science and Engineering, Tianjin University, Tianjin 300350, P. R. China, E-mail: slzhu@tju.edu.cn

immiscible solute elements facilitates the formation of medium-range-ordered atomic configurations, which is primarily attributed to the impeded long-range diffusion.

The clustered glassy alloys have been widely researched, such as Ti-based[6], Fe-based[7–8], and Zr-based[9–15] alloys. In the Zr-based clustered metallic glass system, several components have been developed, including the ZrAlCoAg[12], ZrAlNiCuAg[11,16], and ZrCuNiAlNb[9]. The investigation of $Zr_{65}Al_{7.5}Co_{27.5-x}Ag_x$ ($x$=5–20, at%) and $Zr_{65}$Al7.5Ni10$Cu_{17.5-x}Ag_x$ ($x$=0–17.5, at%) alloys involves the substitution of Ag with the solute elements[11–12], whereas the development of $Zr_{70-x}Cu_{13.5}Ni_{8.5}Al_8Nb_x$ ($x$=0–10, at%) and $Zr_{70-x}Cu_{12.5}Ni_{10}Al_{17.5}Ag_x$ ($x$=0–16, at%) alloys is mainly focused on the replacement of the solvent (Zr) with Nb or Ag[9,16]. XRD patterns of $Zr_{65}Al_{7.5}Co_{27.5-x}Ag_x$ ($x$=5–20, at%) alloy after annealing at the first exothermic peak are similar to those of the as-quenched amorphous alloys[12]. Particularly, icosahedral phase is precipitated in the $Zr_{65}Al_{7.5}Co_{12.5}Ag_{15}$ alloy after annealing at the first exothermic peak. This phenomenon is similar to that of other alloy systems.

In addition, with increasing the concentration of solute atoms, the glass transition temperature ($T_g$) of Zr-based cluster metallic glass is gradually increased, which is beneficial to improve the thermal stability of metallic glass. In the $Zr_{65}Al_{7.5}Ni_{10}Cu_{17.5-x}Ag_x$ ($x$=0–17.5, at%) alloy system, $T_g$ is increased with increasing the Ag concentration, and the alloys with 65at% Zr and 17.5at% Ag show no significant precipitation[11]. For the $Zr_{70-x}Cu_{13.5}Ni_{8.5}Al_8Nb_x$ ($x$=0–10, at%) alloys, the icosahedral phase can be precipitated by annealing at the first exothermic peak with the maximum Nb concentration of 8at%. Besides, $T_g$ is increased with increasing the Nb concentration[9]. In $Zr_{70-x}Cu_{12.5}Ni_{10}Al_{7.5}Ag_x$ ($x$=0–16, at%) alloys, the glass transition phenomenon can be clearly observed, and the main precipitate is the icosahedral phase when Ag concentration reaches 10at%. Both $T_g$ and crystallization temperature ($T_x$) are increased with raising the Ag concentration[16].

In order to investigate the formation mechanism of clustered glassy alloys with high thermal stability, an alloy system, $Zr_{65-x}(Al_{0.21}Ni_{0.29}Cu_{0.04}Ag_{0.46})_{35+x}$ ($x$=0, 7.5, 15.0, 22.5), was developed in this research. This study focused on the thermal properties and crystallization behavior of clustered metallic glasses under different temperature conditions.

## 1 Experiment

The $Zr_{65-x}(Al_{0.21}Ni_{0.29}Cu_{0.04}Ag_{0.46})_{35+x}$ alloys were synthesized by the arc-melting technique under the high-purity argon atmosphere. This method ensured the precise composition control and minimized the impurity introduction. Metallic glass ribbons were obtained by the single roller melt spinning method (VF-RQT50)[17], which had the thickness of approximately 40 μm and the width of 1 mm. Precise preparation of these ribbons could ensure the uniformity and consistency for subsequent analyses.

The microstructure of the alloy ribbons was analyzed by XRD tests (DX-2700BH) with Cu Kα radiation. The thermal stability and crystallization behavior of the alloys were investigated through DSC tests (METTLER TGA/DSC 1). By monitoring the thermal behavior, the stability of metallic glass ribbons and the crystallization kinetics could be analyzed.

Vickers hardness measurements were conducted to evaluate the mechanical properties of the alloy system. The indentation size was measured, and the hardness value was calculated accordingly. These results also provided information about the deformation resistance of metallic glass.

## 2 Results and Discussion

The $Zr_{65-x}(Al_{0.21}Ni_{0.29}Cu_{0.04}Ag_{0.46})_{35+x}$ alloys with $x$=0, 7.5, 15.0, 22.5 are denoted as 65.0Zr, 57.5Zr, 50.0Zr, and 42.5Zr specimens, respectively. The specific composition of $Zr_{65-x}(Al_{0.21}Ni_{0.29}Cu_{0.04}Ag_{0.46})_{35+x}$ ($x$=0, 7.5, 15.0, 22.5) alloys are presented in Table 1. XRD patterns of the as-spun $Zr_{65-x}(Al_{0.21}Ni_{0.29}Cu_{0.04}Ag_{0.46})_{35+x}$ ($x$=0, 7.5, 15.0, 22.5) alloy ribbons are shown in Fig. 1. It can be seen that all patterns have a single broad peak, indicating the amorphous characteristics. Notably, the position of the broad diffraction peak shifts towards higher angles with increasing the solute concentration. This phenomenon suggests the increasing incorporation of solute atoms (Al, Ni, Cu, Ag) into the amorphous phase, leading to the contraction of the first nearest neighbor distance[18]. Consequently, a higher degree of densely packed atomic configuration can be achieved, which hinders the atomic rearrangement and enhances the viscosity of the supercooled liquid. These factors ultimately promote the thermal stability of the supercooled liquid and facilitate the formation of a large supercooled liquid region.

Fig. 2 shows DSC curves of the as-spun $Zr_{65-x}(Al_{0.21}Ni_{0.29}$-

**Table 1 Specific composition of $Zr_{65-x}(Al_{0.21}Ni_{0.29}Cu_{0.04}Ag_{0.46})_{35+x}$ ($x$=0, 7.5, 15.0, 22.5) alloys**

| Specimen | Specific composition |
|---|---|
| 65.0Zr | $Zr_{65}Al_{7.5}Ni_{10}Cu_{1.5}Ag_{16}$ |
| 57.5Zr | $Zr_{57.5}Al_9Ni_{12}Cu_2Ag_{19.5}$ |
| 50.0Zr | $Zr_{50}Al_{11}Ni_{14}Cu_2Ag_{23}$ |
| 42.5Zr | $Zr_{42.5}Al_{12}Ni_{16.5}Cu_{2.5}Ag_{26.5}$ |

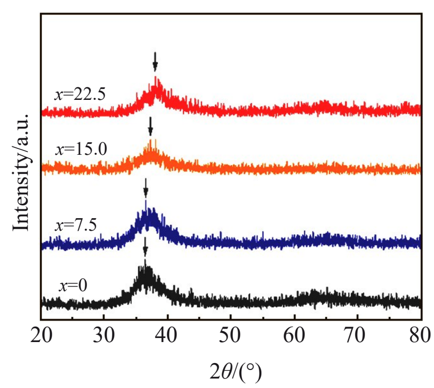


Fig.1 XRD patterns of as-spun $Zr_{65-x}(Al_{0.21}Ni_{0.29}Cu_{0.04}Ag_{0.46})_{35+x}$ ($x$=0, 7.5, 15.0, 22.5) alloy ribbons (arrows indicate the summit positions of main broad peak)

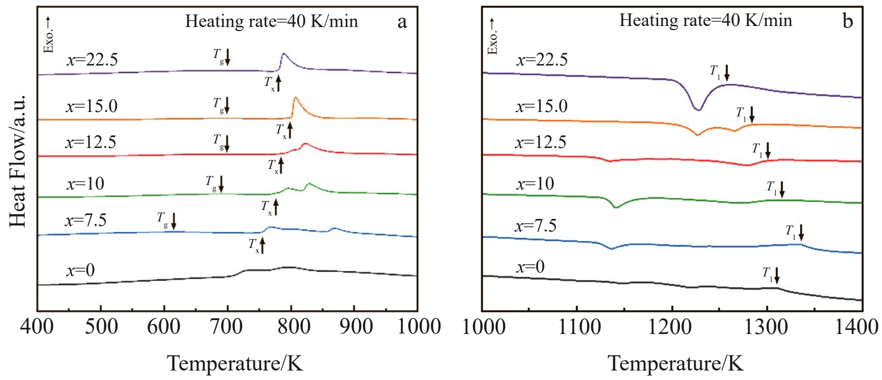


Fig.2 DSC curves of as-spun $Zr_{65-x}(Al_{0.21}Ni_{0.29}Cu_{0.04}Ag_{0.46})_{35+x}$ alloy ribbons under heating rate of 40 K/min: (a) crystallization process and (b) melting process

$Cu_{0.04}Ag_{0.46})_{35+x}$ ($x$=0, 7.5, 10.0, 12.5, 15.0, 22.5) alloy ribbons under the heating rate of 40 K/min. For the 65.0Zr specimen during crystallization process, neither the glass transition nor the supercooled liquid region can be identified, which is similar to the results in Ref. [11]. When $x$=7.5 – 22.5, the supercooled liquid region is reduced with increasing the solute concentration. The decomposition of the glassy phase occurs in two stages and three stages for the 65.0Zr and 57.5Zr specimens. In contrast, the crystallization stage occurs in the 50.0Zr and 42.5Zr specimens. The change in the number of decomposition stages reflects the change in crystallization mode, which is influenced by the primary precipitate phase with different solute concentrations.

In the high temperature range of DSC curves, the endothermic peak indicates the melting process, as shown in Fig.2b. Before the complete melting of the alloys, the number of endothermic peaks is decreased with increasing the solute concentration, suggesting that the 50.0Zr and 42.5Zr specimens have eutectic regions[19–20].

Table 2 shows the thermal properties obtained from DSC curves of Zr-based glassy alloys in this research and other reports. Among the thermal properties, $\Delta T_x=T_x-T_g$ and $T_{rg}=T_g/T_l$. In this research, both $T_g$ and $T_x$ are increased, whereas $\Delta T_x$ is decreased with increasing the solute concentration. It is worth noting that the 57.5Zr specimen exhibits a remarkably high $\Delta T_x$ value of 141 K, which is higher than that of the $Zr_{65}Al_{7.5}Ni_{10}Cu_{17.5}$ alloy, indicating the exceptional thermal stability. $T_l$ is firstly increased and then decreased with increasing the solute concentration. As a result, $T_{rg}$ gradually increases, indicating an improved GFA at higher solute concentrations. The 42.5Zr specimen has a high $T_{rg}$ value of 0.558. Compared with the alloys with good GFA in the formation of bulk metallic glasses, such as $Zr_{65}Al_{7.5}Ni_{10}Cu_{17.5}$[20] and $Zr_{54}Al_{7.5}Ni_{10}Cu_{12.5}Ag_{16}$[16] alloys, all specimens in this research are good glass formers based on their $\Delta T_x$ and $T_{rg}$ values.

The stability of the supercooled liquid phase in metallic glasses is strongly associated with the presence of medium-range-ordered atomic clusters[22]. It is reported that Zr-Al-Ni-Cu-Ag glassy alloys are composed of Zr-Al-Ni and Zr-Al-Cu/Zr-Al-Ag units[11]. Because Ag has a larger atomic size than

**Table 2 Glass transition temperature ($T_g$), crystallization temperature ($T_x$), liquidus temperature ($T_l$), supercooled liquid region ($\Delta T_x$), and reduced glass transition temperature ($T_{rg}$) of different Zr-Al-Ni-Cu-Ag glassy alloys**

| Alloy | $T_g$/K | $T_x$/K | $T_l$/K | $\Delta T_x$/K | $T_{rg}$ | Ref. |
|---|---|---|---|---|---|---|
| $Zr_{65}Al_{7.5}Ni_{10}Cu_{17.5}$ | 622 | 749 | 1180 | 127 | 0.527 | [20] |
| $Zr_{60}Al_{15}Ni_{15}Cu_{10}$ | 690 | 794 | 1225 | 104 | 0.563 | [21] |
| $Zr_{65}Al_{7.5}Ni_{10}Ag_{17.5}$ | - | 701 | 1400 | - | - | [10] |
| $Zr_{56}Al_{16}Ni_{16.8}Ag_{11.2}$ | 713 | 783 | 1285 | 70 | 0.555 | [22] |
| $Zr_{56}Al_{16}Ni1_{9.6}Ag_{8.4}$ | 714 | 791 | 1274 | 77 | 0.560 | [22] |
| $Zr_{65}Al_{7.5}Ni_{10}Cu_{1.5}Ag_{16}$ | - | 701 | 1338 | - | - | [10] |
| $Zr_{65}Al_{7.5}Ni_{10}Cu_{1.5}Ag_{16}$ | - | 703 | 1310 | - | - | This research |
| $Zr_{57.5}Al_{9}Ni_{12}Cu_{2}Ag_{19.5}$ | 614 | 755 | 1335 | 141 | 0.460 | This research |
| $Zr_{50}Al_{11}Ni_{14}Cu_{2}Ag_{23}$ | 701 | 801 | 1295 | 100 | 0.541 | This research |
| $Zr_{42.5}Al_{12}Ni_{16.5}Cu_{2.5}Ag_{26.5}$ | 703 | 782 | 1260 | 79 | 0.558 | This research |
| $Zr_{57}Al_{10}Ni_{8}Cu_{20}Ag_{5}$ | 668 | 779 | 1135 | 111 | 0.589 | [23] |
| $Zr_{54}Al_{7.5}Ni_{10}Cu_{12.5}Ag_{16}$ | 678 | 788 | - | 110 | - | [16] |
| $Zr_{49.5}Al_{18.6}Co_{18.6}Cu_{6.3}Ag_{7}$ | 753 | 806 | 1222 | 53 | 0.616 | [24] |
| $Zr_{48}Al_{8}Cu_{33}Ag_{11}$ | 706 | 770 | 1218 | 64 | 0.580 | [25] |

Cu does, the volume of the Zr-Al-Ag unit is greater than that of the Zr-Al-Cu unit, resulting in the difficult atomic rearrangement within the Zr-Al-Ag unit. Consequently, the supercooled liquid phase consisting of Zr-Al-Ni and Zr-Al-Ag units has lower precipitation rate. Even when the overall solute concentration of the $Zr_{65-x}(Al_{0.21}Ni_{0.29}Cu_{0.04}Ag_{0.46})_{35+x}$ ($x$=0, 7.5, 15.0, 22.5) alloys increases, the number of Cu atoms is still much smaller than that of Al, Ni, and Ag atoms. Thus, the Zr-Al-Ni and Zr-Al-Ag clusters are still the main components in the supercooled liquid phase. Moreover, the Zr-Al-Ni units have stronger bonding effect due to their larger negative heats of mixing between Zr-Ni and Al-Ni pairs[14], thereby promoting the thermal stability of the glassy phase. In the 57.5Zr specimen, the number and proportion of Zr-Al-Ni and Zr-Al-Ag clusters reach the maximum values, leading to the optimal thermal stability. However, with increasing the solute concentration, the Zr concentration in the $Zr_{65-x}(Al_{0.21}Ni_{0.29}Cu_{0.04}Ag_{0.46})_{35+x}$ ($x$=0, 7.5, 15.0, 22.5) alloys is decreased. Therefore, the total number of Zr-Al-Ni and Zr-Al-Ag clusters in the supercooled liquid decreases, indicating the reduction in the stability of the supercooled liquid phase.

Fig.3 presents DSC curves of as-spun $Zr_{65-x}(Al_{0.21}Ni_{0.29}Cu_{0.04}Ag_{0.46})_{35+x}$ ($x$=0, 7.5, 15.0, 22.5) alloy ribbons at different heating rates (10–80 K/min). $T_{p_1}$, $T_{p_2}$, and $T_{p_3}$ are the maximum temperatures corresponding to the first, second, and third exothermic peaks, respectively. DSC curves of 65.0Zr and 57.5Zr specimens have two and three exothermic peaks, respectively, whereas the 50.0Zr and 42.5Zr specimens only have one exothermic peak. Except for the 65.0Zr specimen, substantial difference in $\Delta T_x$ can be observed in all other alloy specimens, indicating the high thermal stability of the supercooled liquid phase.

Fig.4 illustrates the variations of characteristic temperatures under different heating rates for as-spun $Zr_{65-x}(Al_{0.21}Ni_{0.29}Cu_{0.04}Ag_{0.46})_{35+x}$ ($x$=0, 7.5, 15.0, 22.5) alloy ribbons. As shown in Fig. 4a, the glass transition ceases in the 65.0Zr specimen, whereas it reemerges in other three specimens with lower Zr concentrations. $T_g$ is increased gradually with increasing the solute concentration, and the highest $T_g$ value is obtained for the 42.5Zr specimen. As shown Fig. 4b and 4c, $T_x$ and $T_{p_1}$ present the similar variation trends: both $T_x$ and $T_{p_1}$ are significantly increased with increasing the solute concentration.

$T_g$, $T_x$, and $T_{p1}$ of $Zr_{65-x}(Al_{0.21}Ni_{0.29}Cu_{0.04}Ag_{0.46})_{35+x}$ ($x$=0, 7.5, 15.0, 22.5) alloys shift towards higher temperatures with increasing the heating rate. The variation of $T_x$ is closely related to that of $T_g$, leading to the increase in $\Delta T_x$. Therefore, the increase in solute concentration primarily contributes to the increment of all characteristic temperatures. It is widely known that a larger $\Delta T_x$ value indicates a stronger capability of the supercooled liquid to inhibit crystallization, thus reflecting greater thermal stability in the glassy alloy. Thus, increasing the solute concentration is beneficial to hinder the crystallization process.

It should be noted that $T_g$ suddenly drops to 614 K at heating rate of 40 K/min for $Zr_{65-x}(Al_{0.21}Ni_{0.29}Cu_{0.04}Ag_{0.46})_{35+x}$ ($x$=7.5, 15.0, 22.5) alloy ribbons, whereas $T_x$ increases slightly, causing the rapid rise of $\Delta T_x$ to the maximum value of 141 K. This is inconsistent with kinetics of amorphous

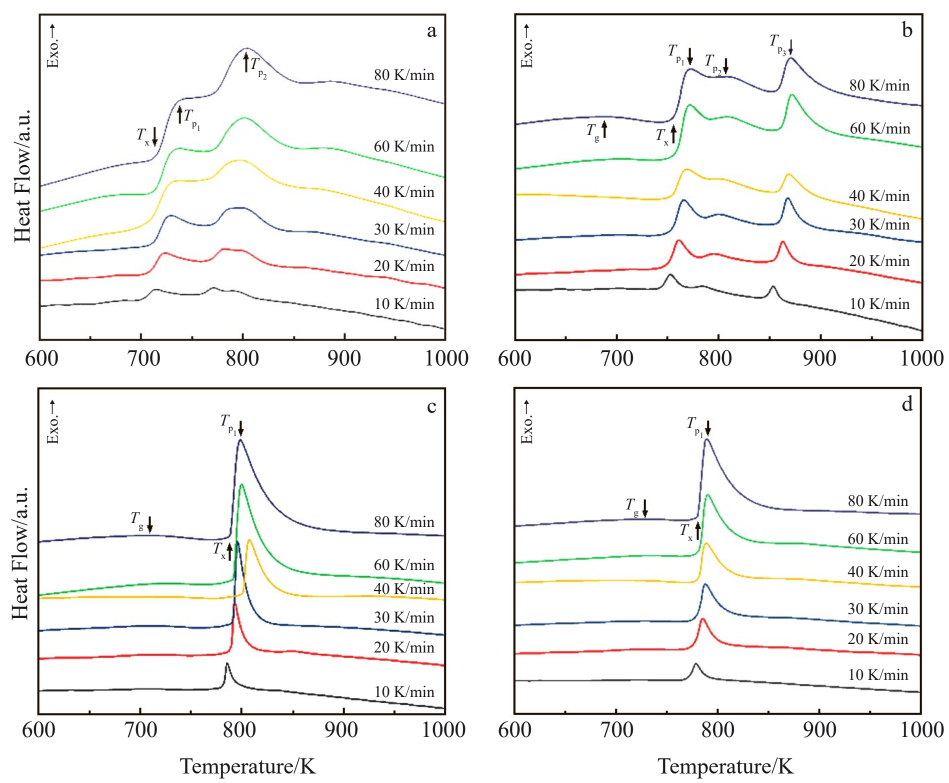


Fig.3 Non-isothermal DSC curves of as-spun $Zr_{65-x}(Al_{0.21}Ni_{0.29}Cu_{0.04}Ag_{0.46})_{35+x}$ alloy ribbons at different heating rates: (a) 65.0Zr specimen, (b) 57.5Zr specimen, (c) 50.0Zr specimen, and (d) 42.5Zr specimen

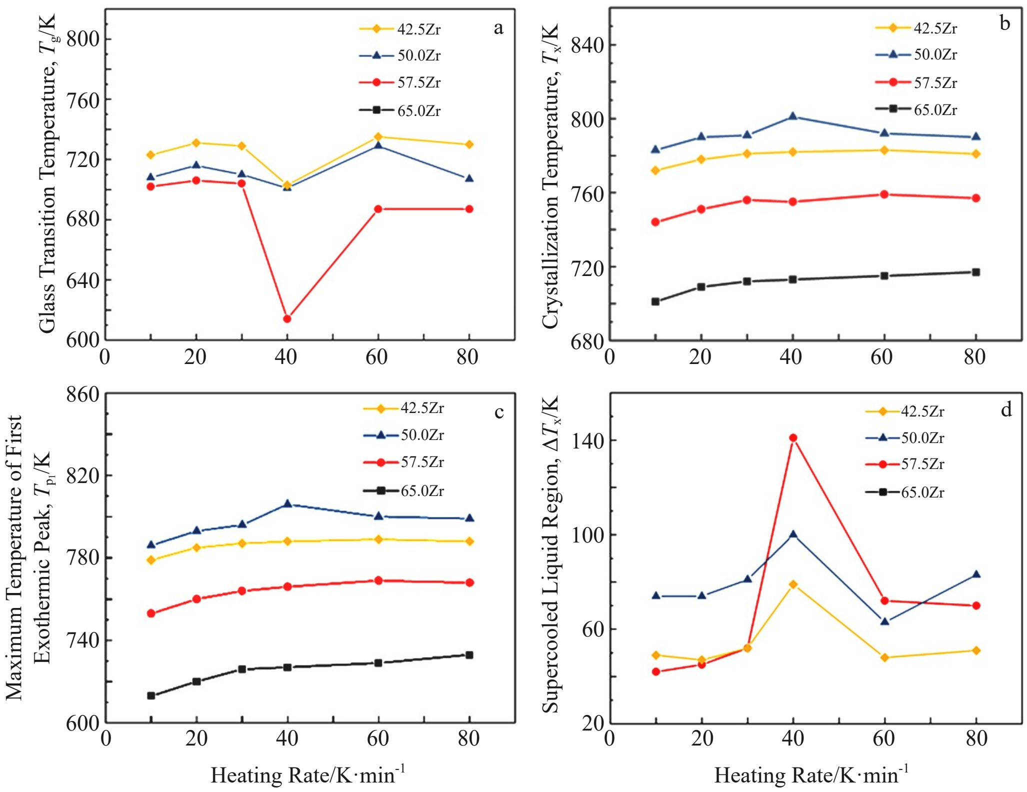

Fig.4 Variation of glass transition temperature $T_g$ (a), crystallization temperature $T_x$ (b), maximum temperature of the first exothermic peak $T_{p_1}$ (c), and supercooled liquid region $\Delta T_x$ (d) under different heating rates of as-spun $Zr_{65-x}(Al_{0.21}Ni_{0.29}Cu_{0.04}Ag_{0.46})_{35+x}$ alloy ribbons

materials. Normally, when the heating rate increases, $T_g$ and $T_x$ should increase accordingly. The experiments were conducted by both METTLER TGA/DSC 1 and NETZSCH STA 449 C instruments to avoid experiment errors. The experiment and simulation results are in good agreement. This phenomenon indicates that the sudden decrease in $T_g$ and the rapid increase in $\Delta T_x$ at heating rate of 40 K/min are objective.

The activation energies of glass transition and crystallization during continuous heating can be calculated by Kissinger equation[23], as follows:

$$\ln\left(\frac{\Phi}{T^2}\right) = -\frac{E}{RT} + C \tag{1}$$

where $\Phi$ represents the heating rate, $E$ denotes the activation energy, $R$ is the universal gas constant, $T$ represents the characteristic temperature ($T_g$, $T_x$, and $T_{p_1}$) corresponding to the glass transition and crystallization processes, and $C$ is a constant. The activation energy ($E_g$, $E_x$, and $E_p$) can be determined by the slope of the Kissinger plots. Fig. 5 shows the Kissinger plots of as-spun $Zr_{65-x}(Al_{0.21}Ni_{0.29}Cu_{0.04}Ag_{0.46})_{35+x}$ ($x$=0, 7.5, 15.0, 22.5) alloy ribbons. The activation energies $E_x$ and growth activation energy $E_{p1}$ associated with the nucleation and growth processes of amorphous alloys[24] are listed in Table 3.

According to the activation barrier energy of the glass transition through Kissinger analysis[25], the variation of the glass transition activation energy is not analyzed through Kissinger plots in this research. Both $E_x$ and $E_{p1}$ activation energies are increased with increasing the solute concentra-

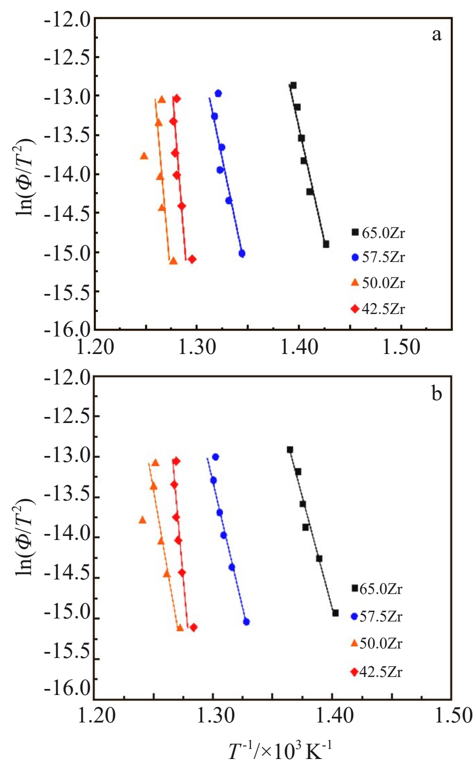

Fig.5 Kissinger plots of as-spun $Zr_{65-x}(Al_{0.21}Ni_{0.29}Cu_{0.04}Ag_{0.46})_{35+x}$ ($x$=0, 7.5, 15.0, 22.5) alloy ribbons: (a) activation energy $E_x$ and (b) growth activation energy $E_{p1}$

**Table 3 Activation energies of $Zr_{65-x}(Al_{0.21}Ni_{0.29}Cu_{0.04}Ag_{0.46})_{35+x}$ ($x$=0, 7.5, 15.0, 22.5) alloy ribbons**

| Specimen | Activation energy, $E_x$/ $kJ \cdot mol^{-1}$ | Growth activation energy, $E_{p1}/kJ \cdot mol^{-1}$ |
|---|---|---|
| 65.0Zr | 60 ± 8 | 52 ± 6 |
| 57.5Zr | 63 ± 9 | 62 ± 3 |
| 50.0Zr | 101 ± 35 | 77 ± 9 |
| 42.5Zr | 89 ± 13 | 101 ± 16 |

tion, indicating the existence of higher barriers for nucleation and growth processes. Fig. 6 presents XRD patterns of the glassy alloy ribbons after annealing for 600 s at the temperatures slightly above the ones corresponding to the first, second, and third exothermic peaks. After annealing at the temperatures above the one corresponding to the first exothermic peak, XRD patterns of 65.0Zr and 57.5Zr specimens are mainly composed of broad peaks, indicating the significant resistance against the primary precipitation and the high thermal stability in the glassy phase.

After annealing at temperatures above the ones corresponding to the second exothermic peaks, it can be seen that the tetragonal $Zr_2Ni$+tetragonal $Zr_2$(Cu, Ag) +hexagonal $Zr_5Al_3$ phases exist in the 65.0Zr specimen, whereas the 57.5Zr specimen consists of tetragonal $Zr_2Ni$, tetragonal ZrAg, and hexagonal $Zr_5Al_3$ phases. Additionally, for the 57.5Zr specimen after annealing at the temperatures above the ones corresponding to the third exothermic peak, a mixed structure consisting of tetragonal $Zr_2Ni$+tetragonal ZrAg+hexagonal $Zr_5Al_3$+tetragonal $Zr_2$(Cu, Ag) phases can be observed. In the 50.0Zr and 42.5Zr specimens, only the single tetragonal ZrAg phase can be detected.

The types of precipitates is increased firstly from three to four and subsequently decreased to one with increasing the solute concentration. The existence of multiple precipitates in the nucleation and growth processes enhances the stability of glassy alloys[26]. Consequently, the 57.5Zr specimen shows the highest thermal stability because it has the most precipitates. This result is consistent with the variations in $\Delta T_x$.

Fig.7 shows XRD patterns of $Zr_{65-x}(Al_{0.21}Ni_{0.29}Cu_{0.04}Ag_{0.46})_{35+x}$ ($x$=0, 7.5) glassy alloys after annealing for 3600 s at the temperatures above the ones corresponding to the first exothermic peaks. With prolonging the annealing duration, XRD peaks of amorphous phase, tetragonal $Zr_2Ni$, tetragonal $Zr_2$(Cu, Ag), and hexagonal $Zr_5Al_3$ phases can be observed in the 65.0Zr specimen. Similarly, the 57.5Zr specimen consists of amorphous phase, tetragonal $Zr_2Ni$, tetragonal ZrAg, and hexagonal $Zr_5Al_3$ phases. This result suggests that the primary precipitation of the 57.5Zr specimen is postponed due to the improved stability of the supercooled liquid phase.

Fig. 8 shows the continuous cooling transformation (CCT) and continuous heating transformation (CHT) diagrams, highlighting significant disparities in the crystallization behavior of these alloys. The cooling curves with labels A, B, and C represent the distinct cooling rates during quenching, whereas label D represents the heating curve during annealing of the amorphous phase. The curve A corresponds to the amorphous ribbons obtained at a rapid cooling rate, and the

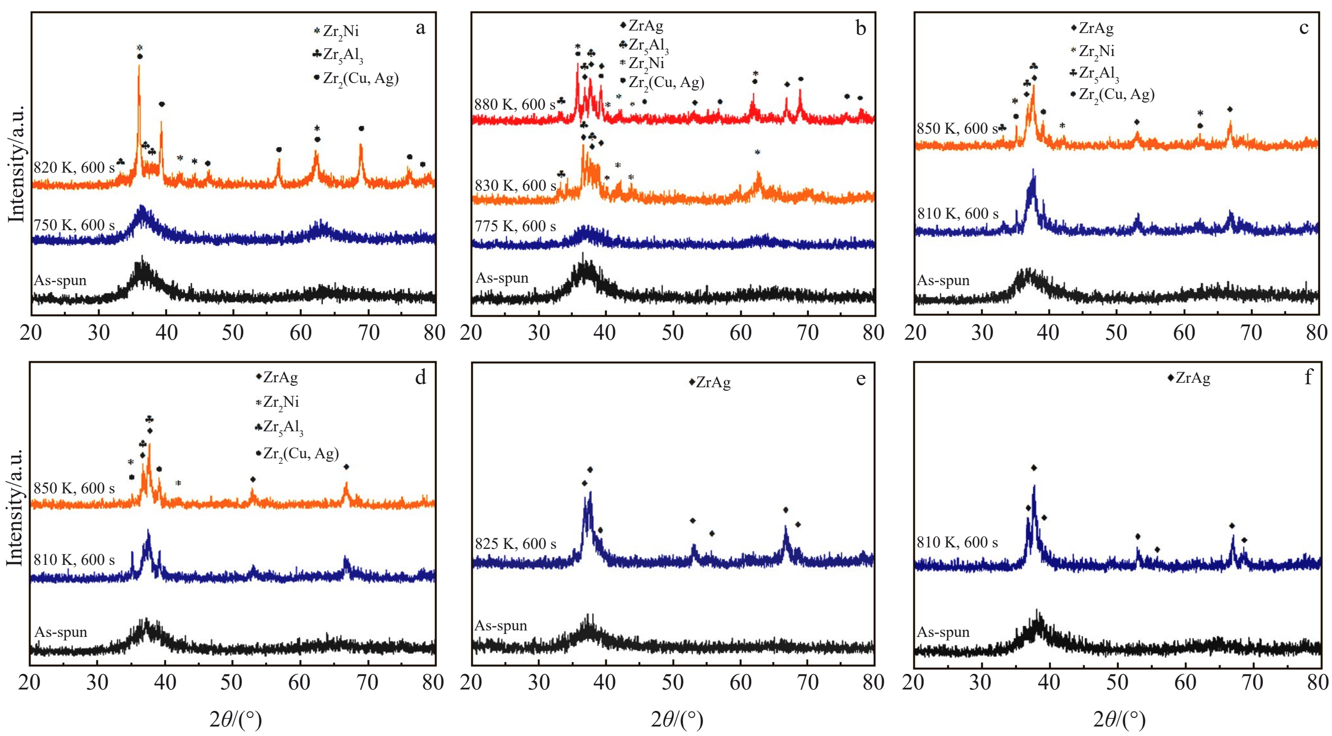


Fig.6 XRD patterns of $Zr_{65-x}(Al_{0.21}Ni_{0.29}Cu_{0.04}Ag_{0.46})_{35+x}$ alloy ribbons after annealing at temperatures above the ones corresponding to different exothermic peaks for 600 s: (a) $x$=0, (b) $x$=7.5, (c) $x$=10.0, (d) $x$=12.5, (e) $x$=15.0, and (f) $x$=22.5

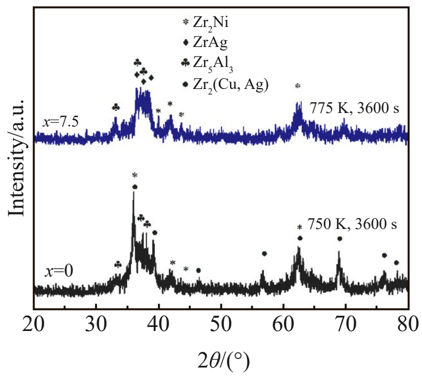


Fig.7 XRD patterns of $Zr_{65-x}(Al_{0.21}Ni_{0.29}Cu_{0.04}Ag_{0.46})_{35+x}$ ($x$=0, 7.5) alloy ribbons after annealing at temperatures above the ones corresponding to the first exothermic peaks for 3600 s

curve D represents the crystalline phase obtained at various temperatures corresponding to the crystallization peaks in Fig. 6. The curves B and C are derived from the curve D. In the $Zr_{65-x}(Al_{0.21}Ni_{0.29}Cu_{0.04}Ag_{0.46})_{35+x}$ ($x$=0, 7.5, 15.0, 22.5) alloys, the ratios of solute atoms (Al, Ni, Cu, and Ag) remain consistent. Thus, the primary variation lies in the proportions of Zr/Al, Zr/Ni, Zr/Cu, and Zr/Ag, as listed in Table 4. Notably, with increasing the solute concentration, the atomic ratio between solvent and solute atoms is decreased. Consequently, a denser atomic configuration and the elevated activation energy barriers can be obtained, and the long-range diffusion, which is vital for solute redistribution and crystalline phase formation, becomes more difficult[27].

The crystallization process was conducted on the glassy ribbons with Zr concentration of 65%[11]. After subsequent annealing at 703 K (slightly above the temperature corresponding to the first exothermic peak) for 600 s, no primary precipitate phase can be observed. Nevertheless, after annealing at 723 K for 3600 s, a combination structure of dispersed phases within the glassy matrix, including the tetragonal $Zr_3Ag$, tetragonal $Zr_2Ni$, and hexagonal $Zr_4Al_3$ phases, can be observed. Additionally, after annealing at 823 K (above the temperature corresponding to the second exothermic peak) for 600 s, the glassy phase completely vanishes, and the tetragonal $Zr_2$(Cu, Ag), tetragonal $Zr_2Ni$, and hexagonal $Zr_5Al_3$ phases can be observed[11]. In this research, the annealing at 750 K for 600 s cannot cause any noticeable precipitation. However, with prolonging the annealing time to 3600 s, the precipitation of tetragonal $Zr_2$(Cu, Ag), tetragonal $Zr_2Ni$, and hexagonal $Zr_5Al_3$ phases can all be observed, even at the temperature below the one corresponding to the second exothermic peak. Furthermore, the broad peaks corresponding to the glassy phase remain unchanged.

Large supercooled liquid region has a significant impact on the phase transition behavior. The primary clusters in the supercooled liquid of $Zr_{65-x}(Al_{0.21}Ni_{0.29}Cu_{0.04}Ag_{0.46})_{35+x}$ ($x$=0, 7.5, 15.0, 22.5) alloys consist of Zr-Al-Ni and Zr-Al-Ag. These clusters facilitate the formation of icosahedral-like medium-range-ordered atomic configurations, which enhance the thermal stability of the supercooled liquid and GFA of the alloys[28]. With increasing the solute concentration, the Zr/Ag ratio gradually reaches to 1, indicating that the composition of the supercooled liquid is close to ZrAg, whereas the residual amorphous phase becomes enriched with Al and Ni elements. Owing to the considerably lower viscosity of the supercooled

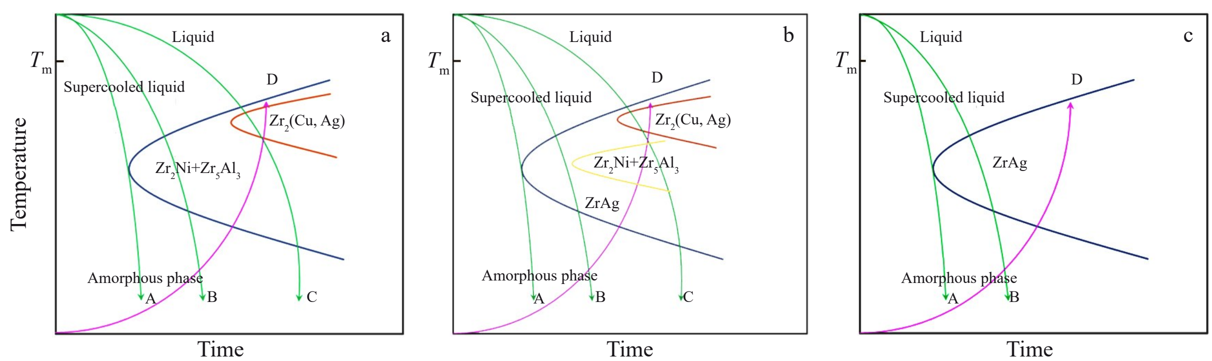


Fig.8 Schematic diagrams of CCT and CHT curves of $Zr_{65-x}(Al_{0.21}Ni_{0.29}Cu_{0.04}Ag_{0.46})_{35+x}$ alloy ribbons: (a) $x$=0; (b) $x$=7.5–12.5; (c) $x$≥15

liquid, compared with the case of the amorphous phase, these alloys exhibit a higher tendency to precipitate the ZrAg phase from the supercooled liquid. Additionally, the positive mixing heat of Ni-Cu, Ni-Ag, and Cu-Ag pairs leads to the repulsive interactions among these elements in the amorphous phase. As a result, the glassy phase presents distinct crystal phases, tetragonal $Zr_2$(Cu, Ag), tetragonal $Zr_2Ni$, and hexagonal $Zr_5Al_3$ phases.

Fig. 9 shows the Vickers hardness of $Zr_{65-x}(Al_{0.21}Ni_{0.29}Cu_{0.04}$-

**Table 4 Atom ratios between solution atom Zr and solute atom Al, Ni, Cu, and Ag of $Zr_{65-x}(Al_{0.21}Ni_{0.29}Cu_{0.04}Ag_{0.46})_{35+x}$ alloy ribbons**

| Specimen | Zr/Al | Zr/Ni | Zr/Cu | Zr/Ag |
|---|---|---|---|---|
| 65.0Zr | 8.67 | 6.50 | 43.33 | 4.06 |
| 57.5Zr | 6.39 | 4.79 | 28.75 | 2.95 |
| 50.0Zr | 4.55 | 3.57 | 25.00 | 2.17 |
| 42.5Zr | 3.54 | 2.58 | 17.00 | 1.60 |

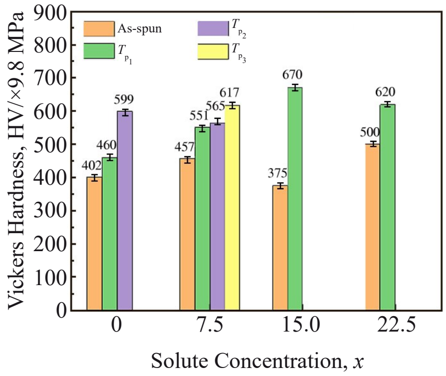


Fig.9 Vickers hardness of $Zr_{65-x}(Al_{0.21}Ni_{0.29}Cu_{0.04}Ag_{0.46})_{35+x}$ ($x$=0, 7.5, 15.0, 22.5) alloy ribbons before and after annealing at different temperatures

$Ag_{0.46})_{35+x}$ ($x$=0, 7.5, 15.0, 22.5) alloy ribbons before and after annealing. $T_{P_1}$, $T_{P_2}$, and $T_{P_3}$ represent the maximum temperatures corresponding to the first, second, and third exothermic peaks. All the alloy ribbons were annealed for 600 s. Initially, the Vickers hardness of the as-spun alloy ribbons increases from 3939.6 MPa to 4478.6 MPa, then decreases to 3675.0 MPa, and finally rises to the maximum value of 4900.0 MPa. Clearly, the hardness is increased with increasing the solute concentration. Although the as-spun alloy ribbons are identified as amorphous material, it should be noted that certain medium-range atom clusters still exist in the glassy matrix[1]. After annealing at the temperature above the one corresponding to the second exothermic peak, these clusters and glassy matrix undergo transformation and change into crystallites. With increasing the solute concentration, the types of precipitates are changed, resulting in the variations of volume fraction and size of these medium-range atom clusters, which leads to hardness change. Subsequently, after annealing at the temperature above the one corresponding to the first exothermic peak for 600 s, the initial favorable bending ductility of $Zr_{65-x}(Al_{0.21}Ni_{0.29}Cu_{0.04}Ag_{0.46})_{35+x}$ ($x$=0, 7.5, 15.0, 22.5) alloy ribbons turns to the brittle state.

The Vickers hardness is rapidly increased with increasing the annealing temperature, particularly after the complete decomposition of the glassy phase. This phenomenon can be attributed to the presence of clusters and nanoscale crystallites, which contribute to the precipitation hardening within the glassy phase of the 65.0Zr and 57.5Zr specimens. Moreover, the precipitation of multiple crystallites, including the tetragonal $Zr_2Ni$, tetragonal $Zr_2(Cu, Ag)$, tetragonal ZrAg, and hexagonal $Zr_5Al_3$ phases, further enhances the hardness of the alloy ribbons. For the 50.0Zr and 42.5Zr specimens, only the tetragonal ZrAg phase is precipitated. But the hardness still rises rapidly.

## 3 Conclusions

1) Increasing the solute concentrations of Al, Ni, Cu, and Ag can shift the summit position of the broad diffraction peaks to the higher angles. The glass transition phenomenon occurs and the supercooled liquid region ($\Delta T_x$) exists in the $Zr_{65-x}(Al_{0.21}Ni_{0.29}Cu_{0.04}Ag_{0.46})_{35+x}$ alloys with $x \geqslant 7.5$.

2) With increasing the solute concentration, the glass transition temperature $T_g$ is increased faster than the crystallization temperature $T_x$, resulting in the gradual decrease in the supercooled liquid region $\Delta T_x$. Conversely, the liquidus temperature $T_l$ is decreased with increasing the solute concentration, leading to the increase in the reduced glass transition temperature $T_{rg}$.

3) The characteristic temperatures $T_g$, $T_x$, and the maximum temperature corresponding to the first exothermic peak $T_{p_1}$ of $Zr_{65-x}(Al_{0.21}Ni_{0.29}Cu_{0.04}Ag_{0.46})_{35+x}$ ($x$=0, 7.5, 15.0, 22.5) alloys shift to higher temperatures with increasing the heating rate. Furthermore, both activation energy $E_x$ and growth activation energy $E_{p1}$ are increased with increasing the solute concentration.

4) The crystallization mode changes from two stages for the $Zr_{65-x}(Al_{0.21}Ni_{0.29}Cu_{0.04}Ag_{0.46})_{35+x}$ alloys with $x$=0 to three stages for the $Zr_{65-x}(Al_{0.21}Ni_{0.29}Cu_{0.04}Ag_{0.46})_{35+x}$ alloys with $x$=7.5, and then decreases to one stage for the $Zr_{65-x}(Al_{0.21}Ni_{0.29}Cu_{0.04}Ag_{0.46})_{35+x}$ alloys with $x$=15.0 and 22.5. The $Zr_{65-x}(Al_{0.21}Ni_{0.29}Cu_{0.04}Ag_{0.46})_{35+x}$ metallic glass with $x$=7.5 possesses a large supercooled liquid region of $\Delta T_x$ of 141 K and high thermal stability, indicating the excellent crystallization resistance.

5) Vickers hardness of $Zr_{65-x}(Al_{0.21}Ni_{0.29}Cu_{0.04}Ag_{0.46})_{35+x}$ ($x$=0, 7.5, 15.0, 22.5) alloy ribbons are increased with increasing the solute concentration, and it is increased rapidly with the variation of precipitates at higher annealing temperatures.

## References


1 Inoue A, Kong F L, Zhu S L *et al*. *Journal of Alloys and Compounds*[J], 2020, 820: 153164

2 Inoue A, Kong F L, Zhu S L *et al*. *Journal of Alloys and Compounds*[J], 2017, 707: 12

3 Inoue A, Kong F L, Zhu S L *et al*. *MRS Bulletin*[J], 2019, 44(11): 867

4 Koga G Y, Travessa D, Zepon G *et al*. *Journal of Alloys and Compounds*[J], 2021, 884: 161090

5 Inoue A. *Acta Materialia*[J]. 2000, 48(1): 279

6 Oak J J, Louzguine-Luzgin D V, Inoue A *et al*. *Materials Science and Engineering C*[J], 2009, 29(1): 322

7 Hirata A, Hirotsu Y, Amiya K *et al*. *Physical Review B*[J], 2008, 78(14): 144205

8 Li X, Makino A, Yubuta K *et al*. *Materials Transactions*[J], 2009, 50(6): 1286

9 Zhu Z W, Gu L, Xie G Q *et al*. *Acta Materialia*[J], 2011, 59(7): 2814

10 Inoue A, Wang Z, Louzguine-Luzgin D V *et al*. *Journal of Alloys and Compounds*[J], 2015, 638: 197

11 Li M M, Inoue A, Han Y *et al*. *Journal of Alloys and Compounds*[J], 2018, 735: 1712

12 Guo Y N, Inoue A, Han Y *et al*. *Journal of Alloys and Compounds*[J], 2019, 783: 545

13 Jin Y, Inoue A, Kong F L *et al*. *Acta Materialia*[J], 2020, 199: 1

14 Wan Y X, Li H S, Chen C J *et al*. *Intermetallics*[J], 2021, 135: 107 233

15 Ding Ruixian, Kou Shengzhong, Li Xiaocheng *et al*. *Rare Metal Materials and Engineering,* 2022, 51(6): 2267 (in Chinese)

16 Zhou W, Hou J X, Zhong Z Z *et al*. *Journal of Non-crystalline Solids*[J], 2015, 411: 132

17 Zhang J Y, Teng X Y, Xu S M *et al*. *Materials Letters*[J], 2017, 189: 17

18 Wang F, Inoue A, Han Y *et al*. *Journal of Alloys and Compounds*[J], 2017, 711: 132

19 Zeng Y Q, Yu J S, Tian Y *et al Acta Materialia[*J], 2020, 200: 710

20 Zhang Q S, Zhang W, Inoue A. *Materials Transactions*[J], 2006, 47(11): 2804

21 Zhang T, Inoue A, Masumoto T. *Materials Transactions, JIM*[J], 1991, 32(11): 1005

22 Saida J, Matsushita M, Zhang T *et al*. *Applied Physics Letters*[J], 1999, 75(22): 3497

23 Kissinger H E. *Analytical Chemistry*[J], 1957, 29(11): 1702

24 Hu X, Qiao J, Pelletier J M *et al*. *Journal of Non-crystalline Solids*[J], 2016, 432: 254

25 Dong Q, Pan Y J, Tan J *et al*. *Journal of Alloys and Compounds*[J], 2019, 785: 422

26 Lu Z P, Liu C T. *Physical Review Letters*[J], 2003, 91(11): 115505

27 Wang Q, Lu J, Gu F J *et al*. *Journal of Physics D: Applied Physics*[J], 2006, 39(13): 2851

28 Matsushita M, Saida J, Zhang T *et al*. *Philosophical Magazine Letters*[J], 2000, 80(2): 79

# 多组元替换Zr-Al-Ni-Cu-Ag金属玻璃的热稳定性和晶化行为

蒲永亮[1]，钱翊齐[1]，刘钰鑫[1]，刘　丛[2]，丁　静[3]，朱胜利[4,5]

(1. 兰州交通大学 材料科学与工程学院，甘肃 兰州 730070)

(2. 河北工业大学 材料科学与工程学院，天津 300130)

(3. 德州学院 能源与机械学院，山东 德州 253023)

(4. 天津大学 材料科学与工程学院，天津 300350)

(5. 天津市材料复合与功能化重点实验室，天津 300350)

**摘　要**：为提高金属玻璃的热稳定性并获得大过冷液相区，研究了成分为$Zr_{65-x}(Al_{0.21}Ni_{0.29}Cu_{0.04}Ag_{0.46})_{35+x}$（$x$=0，7.5，15.0，22.5）的金属玻璃，重点分析了组分浓度对合金热稳定性、热诱导沉淀相以及力学性能的影响。结果表明，随着合金组分浓度的增加，非晶漫散射峰的峰位向更高角度偏移，出现了玻璃转变现象。随着玻璃转变温度（$T_g$）和晶化温度（$T_x$）增加，液相线温度（$T_l$）降低，导致$T_x$和$T_g$之间的温度差（$\Delta T_x$）减小，约化玻璃转变温度（$T_{rg}$）增大。此外，形核激活能（$E_x$）和长大激活能（$E_{p1}$）随着溶质浓度的增加而增加。初晶从四方$Zr_2Ni$、$Zr_2(Cu, Ag)$、ZrAg和六方$Zr_5Al_3$相的组合转变为单一四方ZrAg相，维氏硬度呈现出增加的趋势。通过研究，发现了具有141 K过冷液相区（$\Delta T_x$）和高热稳定性的新型金属玻璃$Zr_{65-x}(Al_{0.21}Ni_{0.29}Cu_{0.04}Ag_{0.46})_{35+x}$（$x$=7.5），且具有较强的抵抗晶化的特性。本研究采用的多组元替换策略对提高金属玻璃的热稳定性具有重要意义。

**关键词**：金属玻璃；热稳定性；晶化行为；微观组织；维氏硬度

作者简介：蒲永亮，男，1987年生，博士，副教授，兰州交通大学材料科学与工程学院，甘肃 兰州 730070，E-mail：puyl@mail.lzjtu.cn